Probing potential energy surfaces with high-resolution spectroscopy

From the Universe's carbon locker to molecular machines

Maltseva, E.O.

Publication date
2017

Document Version
Other version

License
Other

CHAPTER 4

High-resolution IR absorption spectroscopy of polycyclic aromatic hydrocarbons in the 3 μm region: Role of hydrogenation and alkylation

Abstract

In this work we report on high-resolution IR absorption studies on polycyclic aromatic hydrocarbons (PAHs) with extra hydrogens (H-PAHs) and methyl groups (Me-PAHs) in the 3 μm region. We aim to elucidate the spectral changes in the CH-stretch region that result from chemical changes in the molecular periphery. To this purpose, advanced laser spectroscopic techniques combined with mass spectrometry are applied on supersonically cooled 1,2,3,4-tetrahydronaphthalene, 9,10-dihydroanthracene, 9,10-dihydrophenathrene, 1,2,3,6,7,8-hexahydropyrene, 9-methylanthracene, and 9,10-dimethylanthracene allowing us to record mass- and conformationally-selective absorption spectra of the aromatic, aliphatic and alkyl CH-stretches in the 3.175-3.636 μm region with laser-limited resolution. We compare the experimental absorption spectra with standard harmonic calculations and with second-order vibrational perturbation theory anharmonic calculations that use the SPECTRO program for treating resonances. We show that anharmonicity plays an important–if not dominant–role, affecting not only aromatic, but also aliphatic and alkyl CH-stretch vibrations. Combining these advanced calculations with the experimental high-resolution data leads to the conclusion that the variation of Me- and H- PAHs composition might well account for the observed variations in the 3 μm emission spectra of carbon-rich and star-forming regions. Our laboratory studies also suggest that heavily hydrogenated PAHs form a significant fraction of the carriers of IR emission in regions in which an anomalously strong 3 μm plateau is observed.*

*This chapter is adopted from E. Maltseva, A. Petrignani, A. Candian, C. J. Mackie, X. Huang, T. J. Lee, A. G. G. M. Tielens, J. Oomens, W. J. Buma.
Astrophys. J. submitted.

4.1 Introduction

The series of unidentified infrared bands (UIRs) (3.29, 6.2, 7.7, 8.7 and 11.3 μm) observed in a variety of astrophysical environments has puzzled astronomers for decades since their first discovery in 1973.[1,2] The most generally accepted hypotheses is the so-called "PAH hypothesis" which asserts that the UIR emission is a result of radiative cooling of isolated Polycyclic Aromatic Hydrocarbons (PAHs)–a class of organic compounds consisting of hydrogen and carbon atoms combined in fused aromatic rings–that have been excited by UV radiation and, after radiationless decay to the ground electronic state, populate the ground state's vibrational manifold.[3–5] Due to its accessibility with ground-based telescopes, one of the most studied UIR features is the 3.3 μm band that has been attributed to CH-stretch vibrational modes of aromatic hydrocarbons. With higher resolution and sensitivity, observations have revealed that the 3.3 μm band is accompanied by a plateau spanning the 3.1-3.7 μm region (the so-called 3 μm plateau) with superimposed bands at 3.40, 3.46, 3.51, and 3.56 μm. Observations have also demonstrated that there is a great diversity in the relative strengths of these sub-features depending on the nature of the emission source. In the majority of astronomical environments showing UIRs, the 3.29 μm band dominates the 3 μm region.[6,7] However, there are known sources (mostly protoplanetary nebulae) that possess an abnormal 3 μm profile with the plateau and its superimposed bands having the same intensity as the 3.29 μm band or in some cases exceeding it.[8–10]

The identification of the 3 μm features in combination with the observed variety of profiles is a key to a profound understanding of carbon evolution in space. It is therefore a subject of extensive discussions. Several suggestions have been put forward to account for the 3.4, 3.46, 3.51, and 3.56 μm bands. These range from an assignment in terms of hot bands of aromatic CH-stretch transitions ν= 2→1 and 3→2 that are red-shifted due to anharmonicity[11] to invoking alkyl CH-stretch modes in methyl-substituted PAHs (Me-PAHs)[12–14] and aliphatic CH-stretch vibrations of PAHs containing extra hydrogen atoms (H-PAHs).[15–17] Seminal laboratory studies of IR emission in gas-phase UV excited PAHs[18] did not find indications for the presence of CH-stretch ν= 2→1 hot-bands that previously had been suggested to account for the 3.4 μm band.[11] It was thus concluded that the satellite 3 μm features must derive from other carriers. It was also found that the IR emission of H-PAHs is more consistent with astrophysical observations than the IR emission of Me-PAHs.[18] The identification of the carriers of the 3 μm plateau is still subject of speculation. For example, the previously proposed hypothesis that the plateau is a quasi-continuum of overlapping overtones and combination bands of CC-stretch modes in PAHs[19] found only partial support from our recent studies on linear acenes and condensed PAHs.[20,21] In these studies experiments and calculations showed unambiguously that aromatic IR activity is restricted to the 3.17-3.33 μm absorption range and thus another carrier is required to explain IR activity in the region 3.33-3.64 μm. Recent extensive matrix-isolation studies and spectroscopic studies on pellets (as grains)[16,17] concluded that CH-stretches in alkyl and methyl groups attached to the periphery of PAHs are the main candidates for the assignment of the weaker bands in the 3 μm region. However, this claim has thus far not been confirmed due to the lack of high-resolution gas-phase IR spectra of these species.

In previous studies[20,21] we applied IR-UV ion-dip laser spectroscopy combined with mass-selective ion detection on PAHs in molecular jets where the seeded molecules could reach internal temperatures of less than 5 K. Such conditions allow for the recording of conformational- and mass-selected spectra with laser-limited linewidths below 0.1 cm^{-1}.

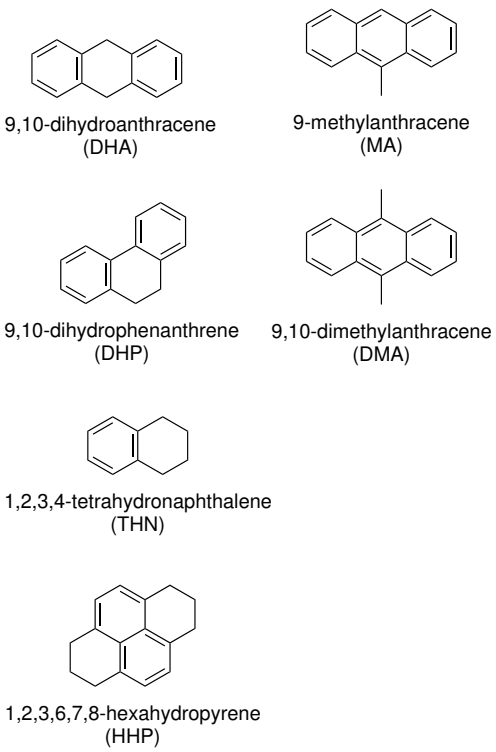

Figure 4.1: Chemical structures of the hydrogenated PAHs DHA, DHP, THN, and HHP, and of the methylated PAHs MA and DMA.

We found that the CH-stretch region of regular PAHs is dominated by large Fermi resonance polyads, which result from a plethora of combination bands, and that a high-end treatment of anharmonic effects including resonance polyads is required to characterize this region computationally. We concluded that the shape of the 3 μm band can act as a spectral signature and help in providing a precise identification of the UIRs carriers.

In the present paper, we extend these high-resolution studies to six more molecules that so far have not been studied in molecular beams: 1,2,3,4-tetrahydronaphthalene (THN) $C_{10}H_{12}$, 9,10-dihydroanthracene (DHA), 9,10-dihydrophenathrene (DHP) $C_{14}H_{12}$, 1,2,3,6,7,8-hexahydropyrene (HHP) $C_{16}H_{16}$, 9-methylanthracene (MA) $C_{15}H_{12}$, 9,10-dimethylanthracene (DMA) $C_{16}H_{14}$ (see Figure 4.1). These decorated PAHs are characterized by the presence of both sp^2 as well as sp^3 hybridized carbon atoms and extend the CH-stretch region from 3.175-3.333 μm to 3.175-3.636 μm. With this work we aim first of all to investigate the role of anharmonicity in the alkyl and aliphatic CH-stretch region and determine whether the plateau in the 3.333-3.636 μm region is primarily due to the effects of anharmonicity. Secondly, we aim to identify the molecular origins of the 3.4, 3.46, 3.51 and 3.56 μm UIR emission bands and of the 3 μm plateau. Finally, we want to establish spectral fingerprints at a molecular–as well as class-sensitive–level for two different classes of decorated PAHs, namely H-PAHs and Me-PAHs. These fin-

gerprints are important since they can help us to shed light on the PAH composition in different astronomical environments.

4.2 Methods

4.2.1 Experimental techniques

The experiments were carried out using a molecular beam setup described earlier.[22] In order to obtain cold and isolated molecules the sample of interest was kept at temperatures above its melting point in the container attached to a pulsed valve (General Valve). Subsequent pulsed expansion in a carrier gas (argon at 2 bars), with a typical pulse duration of 200 μs, resulted in supersonic cooling of the sample molecules.

Double-resonance UV-IR spectroscopy was used to study the ground-state vibrational manifold of PAHs. A two-color resonance enhanced multiphoton ionization (REMPI) scheme was used to create an ion signal that was detected in a time-of-flight spectrometer (R. M. Jordan Co.) at the molecular mass. An excitation laser (Sirah Cobra Stretch) was set to the wavelength of the electronic transitions $S_1 \leftarrow S_1$, well-known from literature (DHA,[23] DHP,[24] THN,[25] HHP,[26] MA,[27] and DMA[28]). An excimer ArF laser (193 nm, Neweks PSX-501) was used for subsequent ionization of the excited molecules. In order to probe IR transitions, an IR laser pulse with a linewidth of 0.07 cm^{-1} was introduced 200 ns prior to the ionization and excitation lasers. The 3 μm beam was produced in a $LiNbO_3$ crystal by difference frequency mixing of the fundamental output of a dye laser (Sirah Precision Scan with LDS 798 dye) and the 1064 nm fundamental of a Nd:YAG laser (Spectra Physics Lab 190). The spectra were recorded in the range of 3.175-3.636 μm (3150-2750 cm^{-1}). With the present S/N ratio, no bands could be observed outside this region.

4.2.2 Computational methods

The present study employs two separate types of calculations to predict the theoretical IR absorption spectra. The first, referred to as G09-h, is the standard harmonic vibrational approach implemented in Gaussian09,[29] while the second, referred to as SP16, is an anharmonic approach which uses both Gaussian09 and a locally modified version of the program SPECTRO.[30] The starting point in both the G09-h and SP16 calculations are density functional theory (DFT) calculations that employ a similar integration grid as in Boese & Martin,[31] the B97-1 functional,[32] and the TZ2P basis set;[33] all of which has been found to give the best performance on organic molecules.[31,34] The quadratic, cubic, and quartic force constants calculated by Gaussian09 are transformed into Cartesian derivatives[35] and serve as input for the SPECTRO program, which performs a vibrational second-order perturbation (VPT2) analysis.[35–37] The SP16 calculations treat the polyads of multiple resonances (modes falling within 200 cm^{-1} of each other) simultaneously and allows for the redistribution of intensity among the resonant modes. A more thorough account of the theoretical aspects of this work is given elsewhere.[38,39]

Complications arise when attempting to treat low barrier "free–rotors" vibrational modes anharmonically[40] such as seen in the methyl groups of the methylated PAHs of this study. As a first approximation we have set the cubic and quartic force constants of these vibrational modes to zero, essentially treating these free–rotor modes as harmonic in the anharmonic analysis.

In the present work vibrational frequencies from the harmonic calculations were scaled with a scaling factor (sf) of 0.96, while anharmonic frequencies did not require any scaling. For further comparison with the experiment both harmonic and anharmonic calculations have been convolved with a 1 and 3 cm^{-1} Gaussian line shape for H- and Me-PAHs, respectively.

4.3 Results

4.3.1 Hydrogenated PAHs

The 3 μm absorption spectra of jet-cooled DHA, DHP, THN, and HHP in the 3.175-3.636 μm (3150-2750 cm^{-1}) region are shown in Fig.4.2(a) - 4.2(d) respectively. The spectra of these molecules display a series of well-separated vibrational bands with linewidths ranging from 1 to 7 cm^{-1}. The positions and relative line intensities are reported in Tables 4.1 and 4.2.

Comparison of these experimental spectra with spectra predicted with the standard harmonic approximation (Fig. 4.2(a)-4.2(d), top panels) appears to give reasonable agreement at first sight. Closer inspection reveals, however, that the distinct features in the 3.420-3.500 μm (2924-2857 cm^{-1}) region are systematically not predicted. Moreover, considerably more bands are observed in the experimental spectra (Tables 4.1 and 4.2) than expected on the basis of the harmonic approximation. The SP16 anharmonic analysis of these molecules (Fig.4.2(a)-4.2(d), middle panels), on the other hand, accounts for resonances and predicts more bands to be IR active. In particular, bands observed in the 3.420-3.500 μm (2924-2857 cm^{-1}) region can now be assigned to the overtones and combination bands of CC-stretch and in-plane CH-bending modes that are coupled to the fundamental aliphatic CH-stretch modes through Fermi resonances (detailed assignments are reported in Mackie et al.[39]).

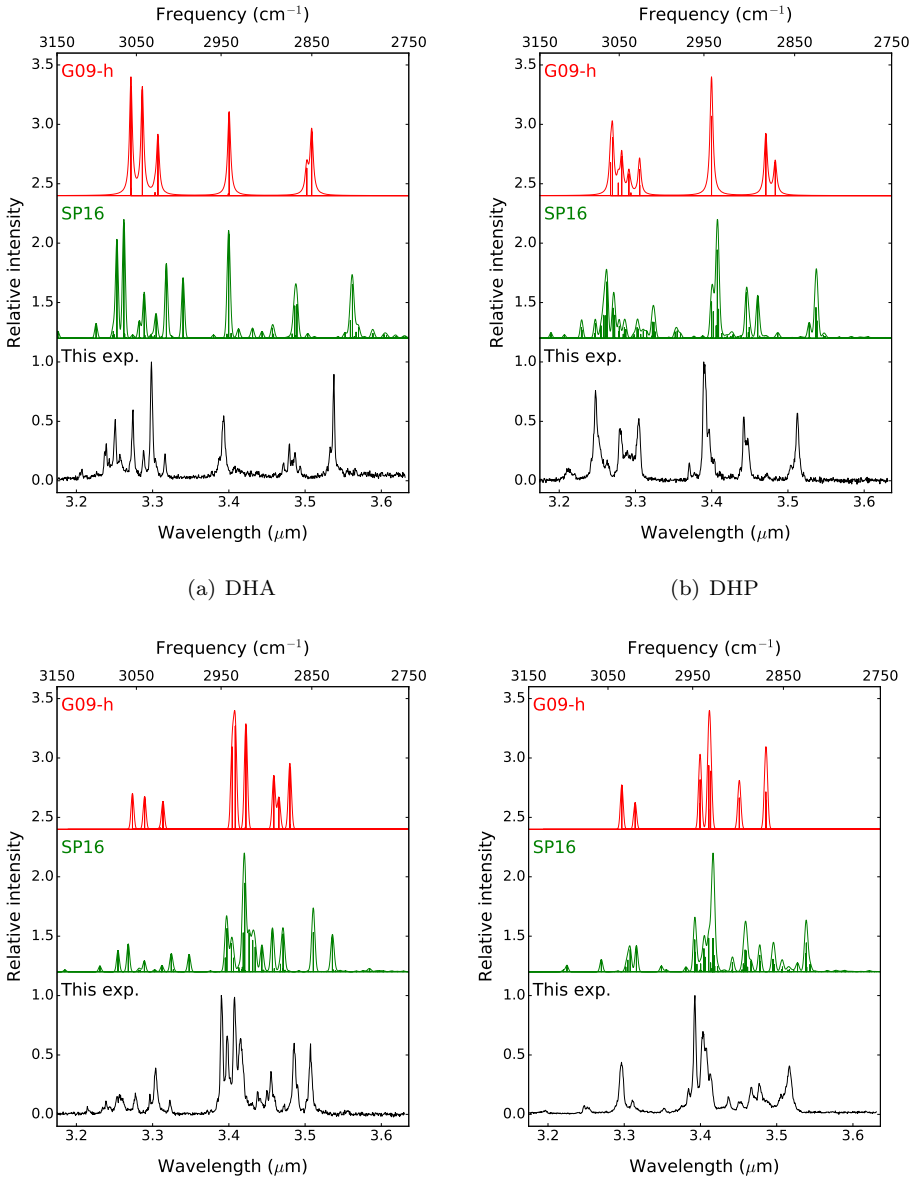

(a) DHA

(b) DHP

(c) THN

(d) HHP

Figure 4.2: IR absorption spectra of DHA, DHP, THN and HHP as predicted by G09-h (scaling factor sf= 0.96) and SP16 calculations (not scaled) together with the molecular beam gas-phase spectrum as measured in the present experiments.

Table 4.1: Experimental line position (cm^{-1}) and relative intensities for the absorption bands of THN, DHA, DHP in 3.175-3.636 μm region.

THN		**DHA**		**DHP**	
freq.	**rel. int.**	**freq.**	**rel. int.**	**freq.**	**rel. int.**
2851.3	0.6	2826.6	0.9	2847.2	0.57
2865.3	0.25	2830.6	0.28	2854.5	0.13
2868.9	0.6	2862.6	0.12	2879.7	0.07
2879.3	0.09	2868	0.24	2901	0.36
2894.2	0.36	2871.1	0.17	2905.1	0.54
2898.8	0.2	2873.8	0.31	2938.3	0.18
2906.5	0.14	2880.2	0.15	2944.3	0.44
2909.2	0.19	2934.2	0.12	2950.2	1
2927.9	0.64	2947	0.55	2966.7	0.15
2934.7	0.99	2951.6	0.2	3026.2	0.52
2942.9	0.66	3015.5	0.23	3034.5	0.23
2949.8	1	3027.1	0.19	3040.1	0.25
3009.5	0.12	3031.7	1	3048.9	0.44
3026.6	0.39	3041.5	0.25	3064.7	0.18
3033.6	0.17	3054	0.6	3079.2	0.76
3051.2	0.18	3070.3	0.22	3084.3	0.19
3066.6	0.14	3075.9	0.52	3112.9	0.1
3070.8	0.17	3083.4	0.19		
3073.6	0.15	3087.1	0.31		
3082.5	0.07	3089.5	0.23		
3087.6	0.1	3099.3	0.08		
3111	0.07	3118.1	0.1		

4.3.2 Methylated PAHs

The absorption spectra of jet-cooled 9-methylanthracene (MA) and 9,10-dimethylanthracene (DMA) are depicted in the bottom panels of Fig. 4.3(a) and 4.3(b), respectively. These spectra feature broad ($\geqslant$6 cm^{-1}) bands, located on a plateau spanning the 3.215-3.484 μm (3110-2870 cm^{-1}) region (see Table 4.2). In contrast to the experiments, the harmonic approximation predicts only two IR active modes in the aliphatic 3.333-3.636 μm (3000-2750 cm^{-1}) region (Fig. 4.3(a),4.3(b), top panels). The SPECTRO VPT2 treatment gives in general a better agreement with the experiment, predicting significantly more bands to be IR active due to Fermi resonances (Figs. 4.3(a),4.3(b), middle panels). The plethora of bands in the anharmonic spectra can account for the plateau observed in the 3.215-3.484 μm (3110-2870 cm^{-1}) region of MA and DMA (detailed assignments are reported in Mackie et al.[39]).

We find that the anharmonic calculations are in reasonably good agreement with the experiment as far as the aromatic region of both molecules is concerned. However, the alkyl region is predicted much better for DMA than for MA. We suspect that restrictions imposed by the higher symmetry of DMA might in part be responsible, but further studies are needed to elucidate this difference. From an analysis of the harmonic and anharmonic results, we find that it is not so straightforward to separate the aromatic region of the spectrum from the alkyl region as could be done for H-PAHs because of the high-frequency methyl CH-stretch vibrations that occur for wavelengths shorter than 3.333 μm (3000 cm^{-1}).

Table 4.2: Experimental line position (cm^{-1}) and relative intensities for the absorption bands of HHP, MA and DMA in 3.175-3.636 μm region.

HHP		**MA**		**DMA**	
rel. int.	**freq.**	**rel. int.**	**freq.**	**rel. int.**	**freq.**
2843.7	0.4	2877.5	0.32	2885.2	0.54
2852.7	0.17	2927.9	0.4	2929.2	0.79
2876.1	0.26	2933.8	0.44	2963.5	0.44
2884.3	0.2	2949.8	0.55	3031.7	0.64
2896	0.1	2965.8	0.3	3057.3	0.55
2910.1	0.15	3001.2	0.3	3078.3	0.92
2930.1	0.34	3020.6	0.58	3092.3	0.83
2934.7	0.56	3037.8	0.7	3102.6	1
2938.3	0.7	3048	0.41		
2947.5	1	3061.5	0.94		
2954.8	0.22	3068.5	0.88		
2982.3	0.05	3072.7	1		
3020.6	0.12	3087.1	0.5		
3033.6	0.44	3092.3	0.43		
3075.5	0.06	3099.3	0.53		
3079.2	0.07				
3128	0.04				

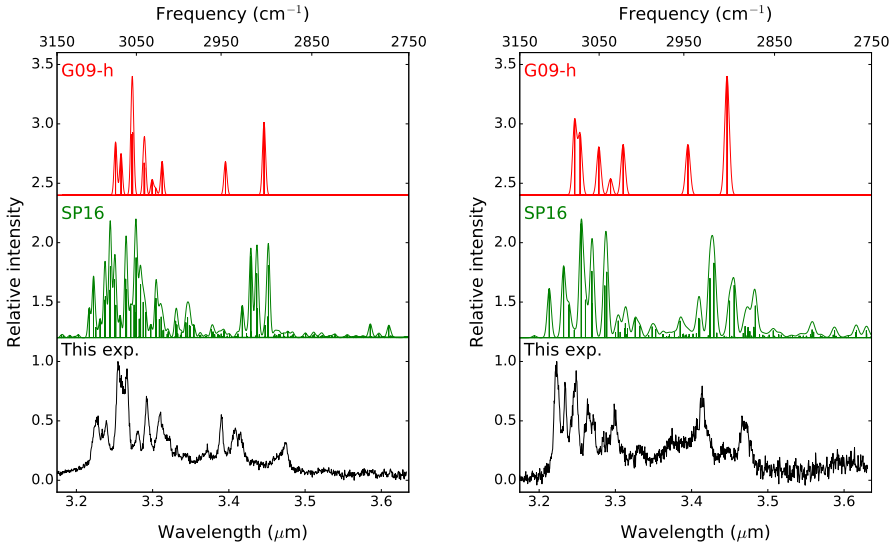

(a) MA

(b) DMA

Figure 4.3: IR absorption spectra of MA and DMA as predicted by G09-h (scaling factor sf= 0.96) and SP16 calculations (not scaled) together with the molecular beam gas-phase spectrum as measured in the present experiments.

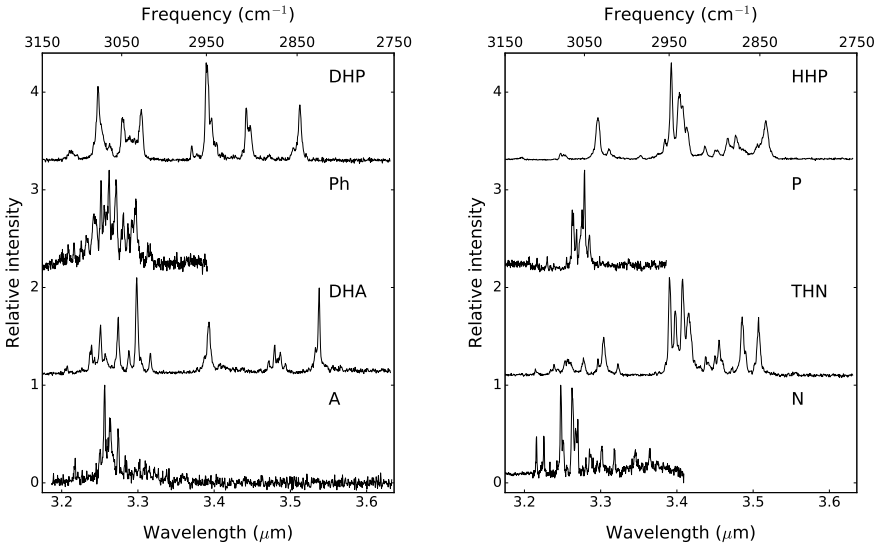

(a) (b)

Figure 4.4: Comparison of IR absorption spectra of jet-cooled (a) A, DHA, Ph, and DHP and (b) N, THN, P, and HHP.

4.4 Discussion

Figs. 4.4(a), 4.4(b), 4.5 show a comparison of IR absorption spectra of the decorated PAHs with the spectra of their bare counterpart PAHs, that is DHA, DHP are compared with anthracene (A) and phenanthrene (Ph); THN, HHP with naphthalene (N) and pyrene (P); and MA, DMA with A. An excess of hydrogens or the presence of a methyl-side group have a strong impact on the CH-stretch region of even minimally decorated PAHs like DHA, DHP and MA. The present study demonstrates that the absorption spectra of these six decorated PAHs in the 3 μm region can in first instance be considered as being built up from two (in case of H-PAHs independent) regions. Their 3.333-3.636 μm (3000-2750 cm^{-1}) region is dominated by the fundamental CH-stretches in the aliphatic or alkyl moieties as well as combination bands and overtones that are coupled with these modes. The 3.175-3.333 μm (3150-3000 cm^{-1}) region, on the other hand, is well known as an aromatic CH-stretch region, although our studies clearly show that this region acquires new properties compared to the CH-stretch region of bare aromatic analogues. In order to understand the spectral changes that the additional hydrogens or methyl-groups promote, several considerations need to be kept in mind.

First, in the case of H-PAHs the presence of additional hydrogens converts a flat aromatic molecule into a bent, mixed aromatic-aliphatic structure with a lower symmetry (for example, D_{2h} for A vs. C_{2v} for DHA). Similarly, the addition of methyl groups introduces asymmetry as some of its hydrogen atoms do not lie in the molecular plane (D_{2h} for A vs. C_s for MA). Such a change in molecular symmetry, along with a larger

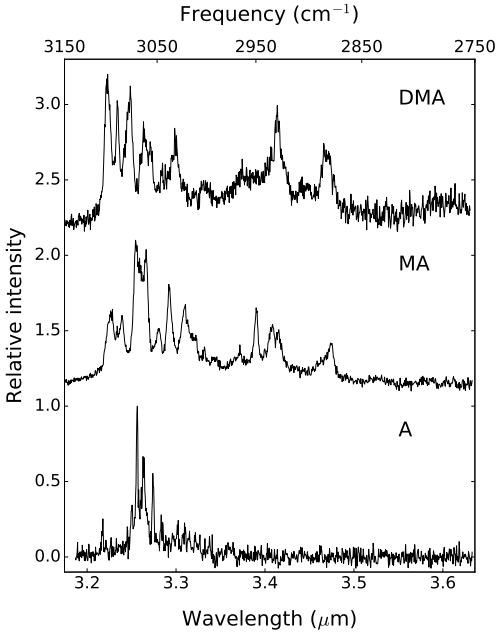

Figure 4.5: Comparison of IR absorption spectra of jet-cooled A, MA and DMA.

number of CH-oscillators increases the total number of normal modes, the number of modes that on symmetry grounds can be IR active, and the number of combination bands that can participate in Fermi resonances.

Second, attachment of additional hydrogens or methyl groups changes the periphery of the parent molecule. In our previous studies we demonstrated that there is a close relation between the shape of the 3.29 μm band and the edge structure of PAHs.[21] In the case of H- and Me-PAHs, we also observe this tendency but it is harder to follow due to the increased complexity of the molecular system. For example, absent solo hydrogens in DMA should result in a weaker activity in the low-energy aromatic region around 3.311 μm (3050 cm^{-1}), but the effect is not visible due to the presence of the sterically hindered methyl stretch at 3.298 μm (3031.7 cm^{-1}) (Fig. 4.5). The steric interactions between the methyl hydrogens and the quartet hydrogens on the ring also strongly affect the high-energy side of the aromatic region around 3.226 μm (3100 cm^{-1}) and lead to frequency that is higher than typically observed for these CH-stretches 3.223 μm (3102.6 cm^{-1}). The presence of the methyl group thus not only changes the number of different types of hydrogens (in this case removing the solo CH-stretch bands from the 3-μm region) but also adds new methyl CH-stretch modes and introduces high-frequency modes similar to the aromatic CH-stretch modes localized in bay-areas of bare PAHs.

Third, for H-PAHs, the changes in the periphery of the molecules affect the aromatic CH-stretches in a similar way as discussed above for Me-PAHs. In DHA, for example, the only aromatic hydrogens are quartet hydrogens since solo positions are hydrogenated.

In our previous studies[21] we showed that solo CH-stretches typically have the lowest frequencies among the various types of aromatic CH-stretches. We thus expect that hydrogenation of A causes, at most, a slight blue shift of the absorption profile of the aromatic CH-stretch band. We observe, in contrast, a red shift of the aromatic band (Fig. 4.4(a)). The harmonic analysis of the fundamental aromatic CH-stretch modes does not show a significant red shift of the pertinent modes and can thus not account for the observed shift. We therefore conclude that the shift originates from the redistribution of the intensity of the fundamental bands in this region over the combination bands via Fermi resonances.

Fourth, apart from the prominent 3.29 μm band attributed to the aromatic CH-stretch vibrations discussed above, we also observe a series of features in the low-frequency region that are associated with the C(sp^3)-H stretch vibrations. The absorption spectra show that these features are very similar as long as the PAHs from the same class (H-PAHs or Me-PAHs). For example, the absorption spectra of hydrogenated species show several well-separated bands restricted to the 3.333-3.636 μm (3000-2750 cm^{-1}) region (Figs. 4.4(a) and 4.4(b)). Careful assignment of these bands on the basis of the anharmonic calculations reveals that the canonical asymmetric aliphatic CH-stretch, which is assumed to be responsible for the interstellar 3.4 μm band, is the strongest in three of the four H-PAHs studied here and very similar in terms of frequency (within 4 cm^{-1}) for all four molecules (DHA 3.393 μm (2947 cm^{-1}), DHP 3.390 μm (2950.2 cm^{-1}), THN 3.390 μm (2949.8 cm^{-1}), and HHP 3.393 μm (2947.5 cm^{-1})). The canonical symmetric aliphatic CH-stretch band, in contrast, is more sensitive to the molecular structure. It shows large variations in intensity and frequencies that are distributed over a much larger range (DHA 3.538 μm (2826.6 cm^{-1}), DHP 3.512 μm (2847.2 cm^{-1}), HHP 3.517 μm (2843.7 cm^{-1}), and THN 3.507 μm (2851.3 cm^{-1})). For Me-PAHs we find that MA and DMA show comparable absorption patterns in the 3.333-3.636 μm (3000-2750 cm^{-1}) regions (Fig. 4.5). The symmetric alkyl CH-stretch gives rise to strong bands at 3.475 μm (2877.5 cm^{-1}) for MA and 3.466 μm (2885.2 cm^{-1}) for DMA, while the asymmetric alkyl CH-stretch is found at 3.409 μm (2933.8 cm^{-1}) and 3.414 μm (2929.2 cm^{-1}) for MA and DMA, respectively, as part of a group of bands in the 3.428-3.356 μm (2917-2980 cm^{-1}) region.

Comparison of the absorption spectra of the heavily hydrogenated HHP and THN with the minimally hydrogenated DHP and DHA leads to the conclusion that hydrogenation causes a rapid increase of the integrated band intensities in the aliphatic region and a decrease in the absorption of aromatic bands. Quantitatively, this is expressed in Fig. 4.6 where the ratio of the integrated intensities of the aliphatic and aromatic CH-stretch bands is plotted as a function of hydrogenation (the ratio of the number of aliphatic and aromatic bonds) for the present set of H-PAHs (black diamonds) together with a set of hot gas-phase spectra of 1,3- and 1,4-cyclohexadiene, cyclohexene, 5,12-dihydronapthacene, 1,2,3,4-tetrahydroanthracene, DHA, DHP, HHP, THN from the NIST catalog[41] (red circles). We note that the present data are completely in line with the independently obtained NIST data that have been measured under completely different conditions. The observed linear relation (Fig. 4.6, blue) is in line with our expectations. Fitting of all data leads to a slope of 1.57$\pm$0.06 which represents the ratio α of aliphatic and aromatic CH-stretch oscillator strengths per CH-bond. This value is in excellent agreement with the value of 1.69 reported in a recent theoretical study.[42]

In view of this good agreement it is surprising that MIS studies of H-PAHs[16] reported a value for α of 2.76, which is significantly higher than concluded here from the gas-phase studies. Further consideration of these results indicates, however, that the difference can

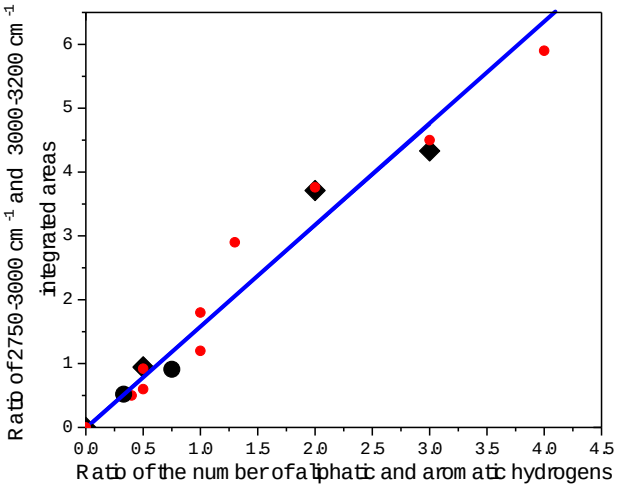

Figure 4.6: Ratio of integrated intensities of the aliphatic (alkyl) and aromatic CH-stretch regions obtained from present experiments (black diamonds for H-PAHs, black circles for Me-PAHs) and from the NIST database (red circles) as a function of the ratio of the number of aliphatic (alkyl) and aromatic bonds in H-PAHs and Me-PAHs. The blue line is a fit to all data.

be traced back to the influence of the environment on band intensities. It has been shown that incorporation of PAHs into rare gas matrices causes a suppression of intensities of IR bands compared to the isolated molecules.[43] Such studies have not been performed for PAHs with aliphatic CH-moieties, but the observation that α obtained in the MIS studies exceeds α observed in gas-phase experiments suggests that aromatic CH-stretch bands are suppressed to a larger extent under rare gas matrix conditions than aliphatic CH-stretch bands. In view of the fact that a large fraction of the spectroscopic data used in astronomical databases have been acquired under MIS conditions, it is clear that further detailed studies on the influence of the environment on band intensities are important for a proper incorporation of these data.

The 3 μm absorption of methylated anthracenes differs significantly in a number of aspects from its hydrogenated analogues (Fig. 4.4(a) and 4.4(b) vs. Fig. 4.5). First of all, unlike H-PAHs, the low-energy side of the aromatic CH-stretch band of Me-PAHs has a contribution from the CH-stretch bands of the methyl group. Secondly, the absorption attributed to the alkyl group starts at 3.484 μm (2870 cm^{-1}), which is 60 cm^{-1} higher than the absorption of hydrogenated PAHs. Thirdly, the absorption spectra of methylated PAHs display broad and poorly separated bands, but even more striking, a prominent plateau that covers the entire 3.215-3.484 μm (3110-2870 cm^{-1}) region. This plateau is a consequence of the high density of accessible states which is caused by the low symmetry and the increased number of normal modes as is confirmed by our anharmonic calculations that show a wide variety of resonances. The plateau can also be

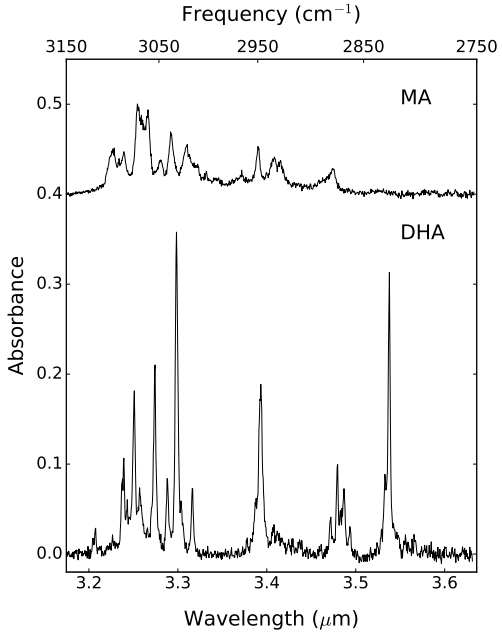

Figure 4.7: Comparison of the experimental IR absorption spectra of jet-cooled DHA and MA.

related to the nearly "free rotor" nature of the methyl groups–and for which the theory cannot account at present.

Fig. 4.7 shows a comparison of the absorbances of DHA and MA instead of the relative scale shown in Figs. 4.2(a) and 4.3(a). A remarkable observation is the difference in the maximum absorption intensity in the two spectra. At the same time, we find that the absorption intensity integrated over the entire spectrum as well as the ratio of integrated intensities of alkyl and aromatic CH-stretches (Fig. 4.6, black circles) is quite similar, and this is indeed what is also predicted by the calculations.[42] From this comparison we thus conclude that the significantly reduced peak intensities of fundamental transitions in the 3 μm region of MA as compared to DHA are due to a redistribution of the intensity over a much larger number of combination bands. This is important as it indicates that for alkylated PAHs peak intensities can in general be expected to be lower than for H-PAHs.

4.5 Astrophysical implications

The present paper has extended our studies of PAHs into the aliphatic and alkyl domains, demonstrating that non-aromatic CH-stretch modes actively participate in Fermi resonances similar to what was previously concluded for aromatic CH-stretches. It is thus clear that anharmonicity and resonances define the shape and the strength of the absorption bands in the 3 μm region and cannot be neglected.

The experimental spectra presented here suggest that the carriers of the 3.4 μm emission band are H-PAHs. We find that the aliphatic asymmetric CH-stretch modes in hydrogenated PAHs are (i) not sensitive to the molecular structure and thereby appear in a restricted frequency range (3.389-3.393 μm (2947.0-2950.2 cm^{-1})), and (ii) amongst the strongest bands as compared to other CH-stretch bands. The asymmetric alkyl CH-stretch of MA and DMA (3.414-3.409 μm (2929-2933 cm^{-1})) also seems to indicate that it is insensitive to structural details. However, in view of the band intensities and bearing in mind that in emission a red shift occurs, the aliphatic asymmetric CH-stretch is more likely to contribute to the 3.4 μm band than the methyl CH-stretch in Me-PAHs. The latter can, however, be responsible for the low-energy shoulder of the 3.4 μm band observed, for example, in IRAS 21282-5050.[14] Our conclusion on the carriers of the 3.4 μm band, however, contradicts with recent theoretical study.[44] Our experimental results supported by previous studies[18] demonstrate that H-PAHs provide a better match to the observed position of the main 3.4 μm band than Me-PAHs and thus suggest that there is an issue with our understanding of the hydrogenation behavior of PAHs in photon-dominated regions.

The symmetric aliphatic CH-stretch shows much more dependence on structural details. Here we find a variation of 25 cm^{-1} in band position (3.538-3.507 μm (2826-2851 cm^{-1})). It might very well be that the astronomically observed 3.51 μm band is due to the overlap of this band for different PAHs. Such a conclusion is supported by the observation of the Orion bar where it was established that the 3.40 and 3.51 μm bands share a common origin.[6,45]

Energetically, the lowest CH-stretch bands of MA and DMA are found at 3.475 μm (2877.5 cm^{-1}) and 3.466 μm (2885.2 cm^{-1}). It is tempting to correlate this band with the 3.46 μm emission band, although the blue shift of the MA and DMA data can at this moment not be explained yet. Further high-resolution spectroscopic studies of a more extensive set of methylated PAHs are in this respect important as they will provide further support for a correlation with the 3.46 μm band. It is well known that the 3.46 μm emission band is more prominent in carbon-rich sources such as the planetary nebula IRAS 21282+5050[46] rather than in the Orion bar or other star-forming regions.[6] The present data thus suggest that the carrier composition in carbon-rich regions contains a significant fraction of methylated PAHs along with hydrogenated ones, while no such abundance of methylated PAHs is expected for ionization regions. At the same time, it must also be noted that in the Orion bar no correlation has been found between an extra component of the 3.40 μm band and the 3.46 μm band.[6] It would be useful to investigate this correlation for other sources like protoplanetary nebulas where these features are more prominent. Another feature observed in a wide range of sources is a band at 3.56 μm. As yet, no conclusive assignment has been made for this band. Our studies, however, suggest that it does not derive from H- and Me-PAHs.

On the basis of our present and previous studies we conclude, supporting IR emission studies,[18] that the plateau extending in the 3.2-3.6 μm region likely has a complex origin, all studied subclasses of molecules being able to contribute to it. The 3.17-3.33 μm region can originate from the overlap of combination bands and overtones coupled to aromatic CH-stretches in bare PAHs, H- and Me-PAHs, and small contributions from the coupling to hindered methyl CH-stretch vibrations. The region 3.33-3.64 μm is fully defined by the IR activity in the aliphatic and alkyl regions of H- and Me-PAHs, although the way they contribute is different. H-PAHs show a series of distinctive bands, while Me-PAHs display a broad absorption plateau with on top low-intensity primary bands.

The ratio of the intrinsic strengths of the aliphatic and aromatic CH-stretch vibrations

($\alpha = 1.58$) obtained in this work allows for a more accurate estimate of the aliphatic fraction. Assuming that the the 3 μm plateau and the satellite features on top of it derive from H-PAHs we estimate that for IRAS 21282+5050 and NGC 1333, IR sources with a normal 3 μm profile, the carriers of the 3 μm emission contain two to three aliphatic hydrogens per eight aromatic hydrogens, while for IR emitters with an anomalously strong 3.4 μm feature the fraction of aliphatic hydrogens is much higher. For IRAS 22272+5435 six to seven aliphatic per eight aromatic hydrogens are found, while for IRAS 04296+3429 the aliphatic hydrogens even outnumber the aromatic hydrogens (more than nine aliphatic per eight aromatic hydrogens). Such estimates contradict recent attempts to quantify the aliphatic fraction by means of MIS studies[16] in which it was concluded that the aromatic moieties exceed aliphatic ones even in anomalous objects like IRAS 04296+3429. On the other hand, the present results corroborate previous gas-phase studies on methyl-coronene where for PAHs in NGC 1333 one methyl side group per eight aromatic hydrogens was estimated.[12]

Finally, we want to emphasize that our studies show that not only the 3.33-3.64 μm region undergoes significant changes upon hydrogenation and/or methylation, but also the region of the aromatic CH-stretch vibrations (3.17-3.33 μm). This has to be taken into account in the analysis of the 3.29 μm band, especially for the sources with a significant intensity of the 3.33-3.64 μm region, as hydrogenated and methylated species are expected to be more present in these sources and contribute to the aromatic region.

4.6 Conclusions

In this paper we have presented high-resolution IR spectra of six jet-cooled decorated PAHs in the 3 μm region. The results of the present study are in line with the conclusions from our previous papers on acenes and condensed PAHs and clearly show that anharmonicity plays an important role in the CH-stretch region of hydrogenated and, in particular, methylated PAHs. In combination with the high density of states this results in a multitude of bands that acquire intensity through Fermi resonances. While for bare PAHs we concluded that anharmonicity can only account for part of the 3 μm plateau, decorated PAHs give rise to plateaus that extend up to over 3.6 μm. A proper treatment of anharmonicity is thus a *conditio sine qua non* for the construction of realistic astronomical models.

Our studies demonstrate that the 3.33-3.64 μm region of hydrogenated and methylated PAHs shows a substantial fraction of intensity which can easily exceed the fraction of intensity associated with the aromatic region. It is therefore very likely that these species are carriers of the low-frequency features in the 3 μm region observed by astronomers. Indeed, we have found that the fundamental symmetric and asymmetric CH-stretches of the methylene part of H-PAHs and of the methyl group of Me-PAHs are remarkably consistent with the 3.4, 3.51, and 3.41, 3.46 μm bands in UIR emission. In order to distinguish between these subclasses, high-resolution studies of the methylene scissoring region (6.9 μm) and the periphery-sensitive CH out-of-plane region (10-15 μm) would be very worthwhile. Such studies are presently in preparation.

References

1. R. M. Merrill, B. T. Soifer, R. W. Russell. *Astrophys. J.*, **200**, 37, 1975.
2. F. C. Gillett, W. J. Forrest, K. M. Merrill. *Astrophys. J.*, **183**, 87, 1973.
3. K. Sellgren. *Astrophys. J.*, **277**, 623, 1984.
4. A. Leger, J. L. Puget. *Astron. Astrophys.*, **137**, 5, 1984.
5. L. J. Allamandola, A. G. G. M. Tielens, J. R. Barker. *Astrophys. J.*, **290**, 25, 1985.
6. G. C. Sloan, J. D. Bregman, T. R. Geballe, L. J. Allamandola, C. E. Woodward. *Astrophys. J.*, **474**, 735, 1997.
7. B. van Diedenhoven, E. Peeters, C. van Kerckhoven, S. Hony, D. M. Hudgins, L. J. Allamandola, A. G. G. M. Tielens. *Astrophys. J.*, **611**, 928, 2004.
8. T. R. Geballe, A. G. G. M. Tielens, S. Kwok, B. J. Hrivnak. *Astrophys. J.*, **387**, L89, 1992.
9. T. R. Geballe, W. E. C. J. van der Veen. *Astron. Astrophys.*, **235**, 9, 1990.
10. M. Goto, S. Kwok, H. Takami, M. Hayashi, W. Gaessler, Y. Hayano, M. Iye, Y. Kamata, T. Kanzawa, N. Kobayashi, Y. Minowa, K. Nedachi, S. Oya, T.-S. Pyo, D. Saint-Jacques, N. Takato, H. Terada, Th. Henning. *Astrophys. J.*, **662**, 389, 2007.
11. J. R. J. Barker, L. J. Allamandola, A. G. G. M. Tielens. *Astrophys. J.*, **315**, 61, 1987.
12. C. Joblin, A. G. G. M. Tielens, L. J. Allamandola, T. R. Geballe. *Astrophys. J.*, **458**, 610, 1996.
13. F. Pauzat, D. Talbi, Y. Ellinger. *Mon. Not. R. Astron. Soc.*, **304**, 241, 1999.
14. M. Jourdain de Muizon, L. B. D'Hendecourt, T. R. Geballe. *Astron. Astrophys.*, **235**, 367, 1990.
15. M. P. Bernstein, S. A. Sandford, L. J. Allamandola. *Astrophys. J.*, **472**, 127, 1996.
16. S. A. Sandford, M. P. Bernstein, C. K. Materese. *Astrophys. J. Suppl. Ser.*, **8**, 1, 2013.
17. M. Steglich, C. Jäger, F. Huisken, M. Friedrich, W. Plass, H.-J. Räder, K. Müllen, Th. Henning. *Astrophys. J. Suppl. Ser.*, **208**, 26, 2013.
18. D. R. Wagner, H. S. Kim, R. J. Saykally. *Astrophys. J.*, **545**, 854, 2000.
19. L. J. Allamandola, A. G. G. M. Tielens, J. R. Barker. *Astrophys. J. Suppl. Ser.*, **71**, 733, 1989.
20. E. Maltseva, A. Petrignani, A. Candian, C. J. Mackie, X. Huang, T. J. Lee, A. G. G. M. Tielens, J. Oomens, W. J. Buma. *Astrophys. J.*, **814**, 23, 2015.
21. E. Maltseva, A. Petrignani, A. Candian, C. J. Mackie, X. Huang, T. J. Lee, A. G. G. M. Tielens, J. Oomens, W. J. Buma 2016. *Astrophys. J.*, **831**, 58, 2016.
22. S. Smolarek, A. Vdovin, A. Rijs, C. A. van Walree, M. Z. Zgierski, W. J. Buma. *J. Phys. Chem. A*, **115**, 9399, 2011.
23. T. Chakraborty, M. Chowdhury. *Chem. Phys. Lett.*, **171**, 25, 1990.
24. T. Chakraborty, M. Chowdhury. *Chem. Phys. Lett.*, **177**, 223, 1991.
25. J. Yang, M. Wagner, J. Laane. *J. Phys. Chem. A*, **111**, 8429, 2007.
26. A. Chakraborty, D. Nath, M. Halder, N. Guchhait, M. Chowdhury. *J. Chem. Phys.*, **114**, 865, 2001.
27. F. Tanaka, S. Hirayama, S. Yamashita, K. Shobatake. *Bull.Chem.Soc.Japan*, **59**,

2011, 1986.

28. S. Hirayama, Y. Iuchi, F. Tanaka, K. Shobatake. *Chem. Phys.*, **144**, 401, 1990.
29. M. J. Frisch, G. W. Trucks, H. B. Schlegel, G. E. Scuseria, M. A. Robb, J. R. Cheeseman, G. Scalmani, V. Barone, B. Mennucci, et al. *Gaussian 09, Rev A.1.*
30. J. F. Gaw, A. Willets, W. H. Green, N. C. Handy. *SPECTRO, version 3.0.*
31. A. D. Boese, J. M. L. Martin. *J. Phys. Chem. A*, **108**, 3085, 2004.
32. F. A. Hamprecht, A. J. Cohen, D. J. Tozer, N. C. Handy. *J. Chem. Phys.*, **109**, 6264, 1998.
33. T. H. Dunning. *J. Chem. Phys.*, **55**, 716, 1971.
34. E. Cané, A. Miani, A. Trombetti. *J. Phys. Chem. A*, **111**, 8218, 2007.
35. C. J. Mackie, A. Candian, X. Huang, T. J. Lee, A. G. G. M. Tielens. *J. Chem. Phys.*, **142**, 244107, 2015.
36. C. J. Mackie, A. Candian, X. Huang, E. Maltseva, A. Petrignani, J. Oomens, W. J. Buma, T. J. Lee, A. G. G. M. Tielens. *J. Chem. Phys.*, **143**, 224314, 2015.
37. A. Candian, C. J. Mackie. *Int. J. Quantum Chem.*, **117**, 146, 2017.
38. C. J. Mackie, A. Candian, X. Huang, E. Maltseva, A. Petrignani, J. Oomens, W. J. Buma, T. J. Lee, A. G. G. M. Tielens. *J. Chem. Phys.*, **145**, 084313, 2016.
39. C. J. Mackie, A. Candian, X. Huang, E. Maltseva,A. Petrignani, J. Oomens, W. J. Buma, T. J. Lee, A. G. G. M. Tielens. *J. Chem. Phys.*, 2017.
40. J. Bloino, M. Biczysko, V. Barone. *J. Chem. Theory Comput.*, **8**, 1015, 2012.
41. E. P. J. Linstrom, W. G. Mallard. *NIST Chemistry WebBook, NIST Standard Reference Database Number 69*, 2017.
42. X. J. Yang, R. Glaser, A. Li, J. X. Zhong. *Astrophys. J.*, **837**, 171, 2017.
43. C. Joblin, L. D'Hendecourt, A. Leger, D. Défourneau. *Astron. Astrophys.*, **281**, 923, 1994.
44. H. Andrews, A. Candian, A. G. G. M. Tielens. *Astron. Astrophys.*, **595**, A23, 2016.
45. T. R. Geballe, A. G. G. M. Tielens, L. J. Allamandola, A. Moorhouse, P. W. J. L. Brand. *Astrophys. J.*, **341**, 278, 1989.
46. M. Jourdain de Muizon, T. R. Geballe, L. B. D'Hendecourt, F. Baas. *Astrophys. J. Lett.*, **306**, 105, 1986.